Geochimica et Cosmochimica Acta, Vol. 69, No. 14, pp. 3619–3630, 2005

0016-7037/05 $30.00 + .00

doi:10.1016/j.gca.2005.02.034

Intense pyrite formation under low-sulfate conditions in the Achterwasser lagoon, SW Baltic Sea

Thomas Neumann,[1,*] Nicole Rausch,[1,†] Thomas Leipe,[2] Olaf Dellwig,[3] Zsolt Berner[1] and Michael E. Böttcher[4]

[1]Institute of Mineralogy and Geochemistry, University of Karlsruhe, D-76128 Karlsruhe, Germany
[2]Institute of Baltic Sea Reasearch Warnemünde, Seestr. 15, D-18119 Rostock, Germany
[3]Institute of Chemistry and Biology of the Marine Environment, Carl von Ossietzky University of Oldenburg, D-26111 Oldenburg, Germany
[4]Max Planck Institute of Marine Microbiology, Department of Biogeochemistry, Celsiusstr. 1, D-28359 Bremen, Germany

(*Received April* 2, 2004; *accepted in revised form February* 21, 2005)

Abstract—In comparison to similar low-sulfate coastal environments with anoxic-sulfidic sediments, the Achterwasser lagoon, which is part of the Oder estuary in the SW Baltic Sea, reveals unexpectedly high pyrite concentrations of up to 7.5 wt%. Pyrite occurs mainly as framboidal grains variable in size with diameters between 1 and 20 μm. Pyritization is not uniform down to the investigated sediment depth of 50 cm. The consumption of reactive-Fe is most efficient in the upper 20 cm of the sediment column, leading to degrees of pyritization (DOP) as high as 80 to 95%.

Sediment accumulation in the Achterwasser takes place in high productivity waters. The content of organic carbon reaches values of up to 10 wt%, indicating that pyrite formation is not limited by the availability of organic matter. Although dissolved sulfate concentration is relatively low (<2 mmol/L) in the Achterwasser, the presence of H_2S in the pore water suggests that sulfate is unlikely to limit pyrite authigenesis. The lack of free Fe(II) in the pore waters combined with the possibility of a very efficient transformation of Fe-monosulfides to pyrite near the sediment/water interface suggests that pyrite formation is rather controlled by (i) the availability of reactive-Fe, which limits the FeS formation, and by (ii) the availability of an oxidant, which limits the transformation of FeS into pyrite. The ultimate source for reactive-Fe is the river Oder, which provides a high portion of reactive-Fe (~65% of the total-Fe) in the form of suspended particulate matter. The surficial sediments of the Achterwasser are reduced, but are subject to oxidation from the overlying water by resuspension. Oxidation of the sediments produces sulfur species with oxidation states intermediate between sulfide and sulfate (e.g., thiosulfate and polysulfides), which transform FeS to FeS_2 at a significant rate. This process of FeS-recycling is suggested to be responsible for the formation of pyrite in high concentrations near the sediment surface, with DOP values between 80 and 95% even under low sulfate conditions.

A postdepositional sulfidization takes place in the deeper part of the sediment column, at ~22 cm depth, where the downward diffusion of H_2S is balanced by the upward migration of Fe(II). The vertical fluctuation of the diffusion front intensifies the pyritization of sediments. We suggest that the processes described may occur preferentially in shallow water lagoons with average net-sedimentation rates close to zero. Such environments are prone to surficial sediment resuspension, initiating oxidation of Fe-sulfides near the sediment/water interface. Subsequent FeS_2 formation as well as postdepositional sulfidization leads to a major pyrite spike at depth within the sediment profile.

1. INTRODUCTION

Pyrite is the most common authigenic sulfide mineral in marine and lacustrine sediments. Its formation takes place via sulfate reduction in anoxic sediments, in the water column of euxinic basins (e.g., Raiswell and Berner, 1985; Wilkin et al. 1996) and in active hydrothermal systems (e.g., Vaughan and Craig, 1978).

The biologic process in low-temperature sedimentary environments is the result of the oxidation of organic matter that occurs through bacterial reduction of sulfate and the production of hydrogen sulfide. In pore waters with pH values above 7, HS^- is the dominant species and reacts with iron from detritus or other sources to form amorphous Fe-S precipitates. Many experiments have shown that an oxidant is required to produce pyrite from precursor iron monosulfides. Aqueous sulfur species with oxidation states intermediate between sulfate and sulfide, for example thiosulfate and polysulfides, may be sufficiently abundant in pore waters to form pyrite from iron monosulfides (Berner, 1970; Rickard, 1975; Berner and Raiswell, 1984; Luther, 1991; Wilkin and Barnes, 1996; Ricard et al. 1995). However, replacement reactions of iron monosulfides can also be viewed in terms of Fe loss from the precursor (Schoonen and Barnes, 1991a; Wilkin and Barnes, 1996; Benning et al. 2000). Experiments carried out by Wilkin and Barnes (1996) indicate that the rate of conversion from iron monosulfides to pyrite is not only a function of solution chemistry, but also depends on the surface oxidation state of precursor iron monosulfides. The most common phases of the Fe-S sequence are formed from "amorphous FeS" transforming into mackinawite (FeS), greigite (Fe_3S_4), and finally pyrite (cubic FeS_2) (Morse et al., 1987). In addition to this sequence, Rickard (1997) showed pyrite formation from H_2S oxidation by iron monosulfides in aqueous solution.

In normal marine sediments (those deposited in O_2-contain-

* Author to whom correspondence should be addressed (thomas.neumann@img.uka.de).
† *Present address:* Institute of Environmental Geochemistry, University of Heidelberg, Im Neuenheimer Feld 236, D-69120 Heidelberg, Germany

ing environments), pyrite formation is limited by the amount and reactivity of organic matter buried in the sediment (Berner, 1984). In most marine pyritic sediments, black FeS is not found at greater depth, indicating essentially complete transformation to pyrite (Berner, 1970). Observations from both modern and ancient settings suggest that, in many cases, the highest extents of Fe-mineral sulfidization are found in euxinic basins with water containing hydrogen sulfide (Raiswell et al. 1988; Lyons and Berner, 1992) where pyrite accumulates in sediments at concentrations up to 5 to 10 wt%.

In contrast to normal marine sediments, the potential for pyrite formation in coastal systems is generally limited by the availability of sulfate, and pyrite concentrations typically reach 0.5 to 2 wt% (Aplin, 2000). Sediments from coastal lagoons and bays are often anoxic-sulfidic sites where intense pyrite production occurs due to relatively high labile organic matter contents and moderate to high H_2S concentrations. One such site is the Baffin Bay, Gulf of Mexico, where pyrite concentrations reach ~1 wt% and the degree of iron pyritization (DOP) (Berner, 1984) is up to 80% (Huerta-Diaz and Morse, 1992). Pyrite formation in estuarine sediments is often an important environmental issue, because pyrite serves as a sink for many discharged heavy metals (Huerta-Diaz and Morse 1992). Especially in highly industrialized areas that include metal mining, such as the Oder catchment, rivers become stressed by anthropogenic input of heavy metals (Pohl et al., 1998).

Estuarine sediments of the river Oder far exceed the typical range of pyrite content (Neumann et al., 1998). Pyrite reaches concentrations of ~5 wt% within the whole Oder estuary. Exceptionally high pyrite concentrations (up to 7.5 wt%) and DOPs of 95% are found in surficial sediments of the Achterwasser, a small basin located in the outer part of the Oder estuary with low sulfate concentrations (< 2 mmol/L). Until now, pyrite formation in low sulfate estuaries with oxic water/sediment interfaces has not been reported to lead to such high FeS_2 concentrations. In this paper, we discuss pyrite authigenesis in the Achterwasser and propose a model for intense pyrite formation in estuarine sediments under low sulfate conditions.

2. REGIONAL SETTING

The Oder estuary is situated in the south-western Baltic Sea at 54°N and 14°E. This area is not a real estuarine system because the river Oder enters the open Baltic Sea through a series of shallow water lagoons (Fig. 1). This results in different hydrochemical conditions, such as salinity and nutrient supply, within the various lagoons of the Oder system (Leipe et al., 1998). The Achterwasser is one of the lagoons of the Oder estuary and covers an area of ~80 km^2 with an average water depth of 3 m (max. 5.5 m). To the northeast, the island Usedom separates the Achterwasser from the open Baltic Sea and to the west the Achterwasser is connected to the estuarine waters of the river Oder.

The water exchange between the Baltic Sea and the Achterwasser depends strongly on sea level changes within the Southern Baltic Sea (Lampe, 1993). During normal sea level conditions, the river Oder fills the Achterwasser with fresh water. During high tides of up to 1 m above normal sea level within the Southern Baltic Sea, brackish Baltic water flows into the

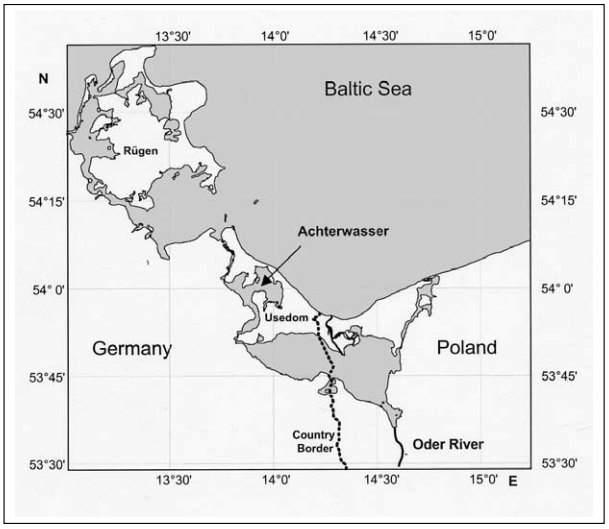

Fig. 1. Location map showing the Achterwasser lagoon within the Oder estuary area, Southern Baltic Sea. An arrow marks the sampling location.

Achterwasser, increasing the salinity from ~1 to ~5 (Al-Ahmad, 1990). Because of the semienclosed situation of the Achterwasser, the saline water can stay there for some months before the fresh water flow of the river Oder decreases the salinity again to normal fresh water conditions (Lampe, 1993).

Furthermore, the Achterwasser is characterized by a high input of nutrients, suspended particulate matter (SPM) and heavy metals via the river Oder (Neumann et al., 1996; Leipe et al., 1998; Pohl et al., 1998). As a consequence, the trophic status of the Achterwasser can be described as eutrophic, and the average annual net primary production of organic matter was found to be 340 g C/m^2. Increased rates of photosynthesis during algae blooms leads to an over-saturation of oxygen in the water column most of the year, but rapid oxygen depletion due to organic matter mineralization below the sediment-water interface results in anoxic conditions in sediments (Neumann et al., 1998).

3. MATERIALS AND METHODS

3.1. Sampling Procedures

This study is based on surface sediments from the Achterwasser retrieved during cruises with R/V Bornhöft in May and October 2000. Individual analytical data for the cruises are presented in electronic annex EA-1-1. The sediment cores were collected at GPS position 13° 57.66′ E, 54° 00.67′ N at a water depth of 4.3 m (Fig. 1). The sediment cores were taken by a Niemistö corer that enables sampling of bottom water, an undisturbed sediment surface, and 40 to 60 cm of underlying sediment (Niemistö, 1974). Sediment cores were sliced into 1 and 2 cm thick discs, freeze-dried and ground in the lab for analyses of bulk chemistry and mineral composition.

Pore water sampling was done on companion cores as follows: Sediment cores within the liners were transferred into a glove box, flushed with nitrogen gas to prevent oxidation, and sliced into 1 cm discs. After centrifuging the sediment samples, the supernatant water was filtered through 0.2 μm cellulose acetate membranes. Aliquots for metal analyses were acidified by nitric acid. For sulfur isotope measurements, the dissolved sulfate was quantitatively precipitated from solution as $BaSO_4$ by the addition of $BaCl_2$ solution and HCl.

3.2. Sediment Analysis

The mineralogical compositions of the sediment samples were analyzed on bulk samples for quartz, feldspar, carbonates, pyrite and after special treatment of the fine fraction (<2 μm), for clay minerals using a Philips PW 1830 powder X-ray diffraction device. Sample treatment and evaluation of spectra was performed using standard procedures described in detail by Gingele and Leipe (1997).

For major and trace element measurements the sediment samples were digested completely in closed PTFE autoclaves (Heinrichs et al., 1986) at 180°C in a mixture of HNO_3, $HClO_4$ (purified by subboiling distillation) and HF (suprapure). Al, Ca, Ti, and Mn were analyzed by ICP-OES (Perkin Elmer Optima 3000XL), while Cd, Ce, Mo, Pb, Sr, Tl, U, and V were determined by ICP-MS (Finnigan MAT Element). $^{206}Pb/^{207}Pb$ isotopic ratios were determined by ICP-MS (Finnigan MAT Element) on total digestions of 14 sediment samples after diluting Pb concentrations to ~5 $\mu g\ l^{-1}$. No mass bias correction was necessary since the instrument was tuned to give best accuracy for the NIST-Standard SRM 981. Total aquisition time was 3 min, consisting of 60 scans. Precision and accuracy were checked by parallel analysis of international reference materials (GSD-3, GSD-5, GSD-6) (Govindaraju, 1994) and SRM 981 (National Institute of Standard and Technology).

Total carbon (TC) and total sulfur (TS) measurements were obtained on split samples with a CS analyzer (Leibold-Heraeus, CA 302). Total organic carbon (TOC) contents were measured using the same procedures on samples that had been treated with 3 N HCl to remove carbonate according to the method described by Schelske and Hodell (1991). Total Fe concentrations in sediments were measured with flame-AAS (Perkin Elmer 1100 B, detection limit of 5 μmol/g) after total dissolution of samples with HNO_3-HF-$HClO_4$. To separate reactive-Fe from pyrite-Fe the following leaching procedure was applied (Huerta-Diaz and Morse, 1990):

1. The *reactive fraction* comprises amorphous and crystalline Fe- and Mn-oxyhydroxides, carbonates, and hydrous alumosilicates, as well as FeS and is obtained after leaching the freeze-dried sediment samples with 1M HCl for 16 h.
2. The *silicate fraction* comprises clay minerals and is extracted after two consecutive leachings with 10M HF for 1 and 16 h, respectively; followed by addition of boric acid to dissolve precipitated fluorides.
3. The *organic fraction* comprises the organic matter that was not decomposed during HCl and HF treatment and is obtained after digestion of the residue with concentrated H_2SO_4 for 2 h. This step is necessary if the sediments contain high amounts of organic matter (> 3 wt%).
4. The *pyrite fraction* is obtained after digestion of the residue with concentrated HNO_3 for 2 h.

In the reactive and the pyrite fraction, Fe was quantified using HR-ICP-MS (VG Elemental, Axiom). To ensure analytical accuracy, certified reference materials were measured (SDO-1 Ohio Shale and SGR-1 Green River Shale) (Govindaraju, 1994). To estimate the extent to which reactive Fe has been converted to pyrite, the degree of pyritization (DOP) was calculated according to Berner (1970):

$$DOP(\%) = (Fe_{pyrite}/(Fe_{pyrite} + Fe_{reactive})) \cdot 100 \quad (1)$$

where pyrite-Fe (fraction 4) is the iron present as pyrite, and reactive-Fe (fraction 1) is the iron that has not reacted to pyrite.

3.3. Pore Water Analysis

Immediately after retrieval of the sediment cores, pH and H_2S concentration were measured at the site of collection with a pH glass electrode (WTW) and an amperometric H_2S electrode (WT 573-H_2S-SX). The pH probe was calibrated with standard WTW buffer solutions at pH 7.0 and 10.0. The sensors were pushed into the sediment core in 1 cm steps. Every 5 cm the upper part of the sediment core was cut off and removed. Measurements of pH carried out in May and in October 2000 showed almost identical results (EA-1-2). Chloride and sulfate contents in the pore water samples were determined by ion chromatography (DX 100, Dionex) with a precision <2%. Iron and Mn was analyzed by HR-ICP-MS (VG Axiom, detection limit 0.1 μmol/L).

Sulfur isotope analyses were performed using precipitated $BaSO_4$ (cf. section 3.1). Sulfur isotope ratios, $^{34}S/^{32}S$, were measured by combustion isotope ratio mass spectrometry (e.g., Böttcher et al., 2001). The cleaned and dried precipitates were combusted to SO_2 in Sn cups with an excess of V_2O_5 in a Carlo Erba EA1108 elemental analyzer coupled to a Finnigan MAT 252 mass spectrometer via a Finnigan MAT Conflo II split interface.

3.4. Pore Water Equilibrium Calculations

Saturation indices (SI) with respect to amorphous FeS (FeS_{am}) and mackinawite (FeS) were calculated using measured pore water pH and concentrations of Fe^{2+} and H_2S as follows:

$$FeS(s) + H^+(aq) \leftrightarrow Fe^{2+}(aq) + HS^-(aq) \quad (2)$$

and

$$\text{ion activity product (IAP)} = \{Fe^{2+}\} \cdot \{HS^-\}/\{H^+\} \quad (3)$$

where $\{Fe^{2+}\}$ is the activity of dissolved ferrous iron and $\{H^+\}$ is the activity of H^+ ions. The pH value cannot necessarily be directly equated to the activity of the hydrogen ion, but it is usually a good approximation to this quantity, being within 0.03 pH for solutions of low ionic strength (Davison and Harbinson, 1988). Activities of HS^- were calculated from measured $H_2S(aq)$ activities, the ambient pH value, and a pK of 6.9 for bisulfide formation from H_2S (Stumm and Morgan, 1996). The distribution of major ferrous iron species ($[Fe^{2+}]$, $[Fe(OH)^+]$, $[Fe(OH)_{2aq}]$, $[FeCl^+]$) were calculated with the computer program *ChemEQL 2.0* (Müller, 1996). Activities of Fe^{2+} were calculated by correcting the Fe^{2+} concentration by the activity coefficient f using the Davies equation (Stumm and Morgan, 1996). An average ionic strength of 0.04 mol/L was calculated from an average Achterwasser salinity of 2. Accordingly, the activity coefficient is 0.48 for divalent ions. Details on the calculation of ferrous iron species and saturation indices are presented in EA-2.

Solubility products (K_{SP}) for FeS minerals were taken from Davison (1991)

$$\text{Amorphous FeS:} K_{SP-Fe(am)} = \{Fe^{2+}\} \cdot \{HS^-\}/\{H^+\} = 10^{-2.95} \quad (4)$$

$$\text{Mackinawite:} K_{SP-Mackinawite} = \{Fe^{2+}\} \cdot \{HS^-\}/\{H^+\} = 10^{-3.60} \quad (5)$$

The saturation index was then calculated as follows:

$$SI = \log(IAP) - \log(K_{SP}) \quad (6)$$

SI >0 indicates supersaturation with respect to FeS minerals, whereas SI <0 indicates undersaturation.

4. RESULTS

4.1. Sediments

Surficial sediments of the Achterwasser can be subdivided into three different types of sediment layers. Below the sediment/water interface a 3 cm thick light brown fluffy, oxic layer occurs (Unit I). This overlies a 20 cm thick soft, black anoxic layer (Unit II), above a dark gray-green mud (Unit III). As a result of intense mixing of the surface sediments by bioturbation and/or strong bottom water currents during heavy storms there is usually no preservation of fine-scaled depositional structures such as lamination within these units (Leipe et al., 1998).

Based on X-ray diffraction data the main mineral assemblage consists of feldspar, quartz and clay minerals. Additionally, calcite and pyrite are present within all units while dolomite and gypsum are found in trace amounts in units II and III only. Scanning electron microscope (SEM) investigations show that

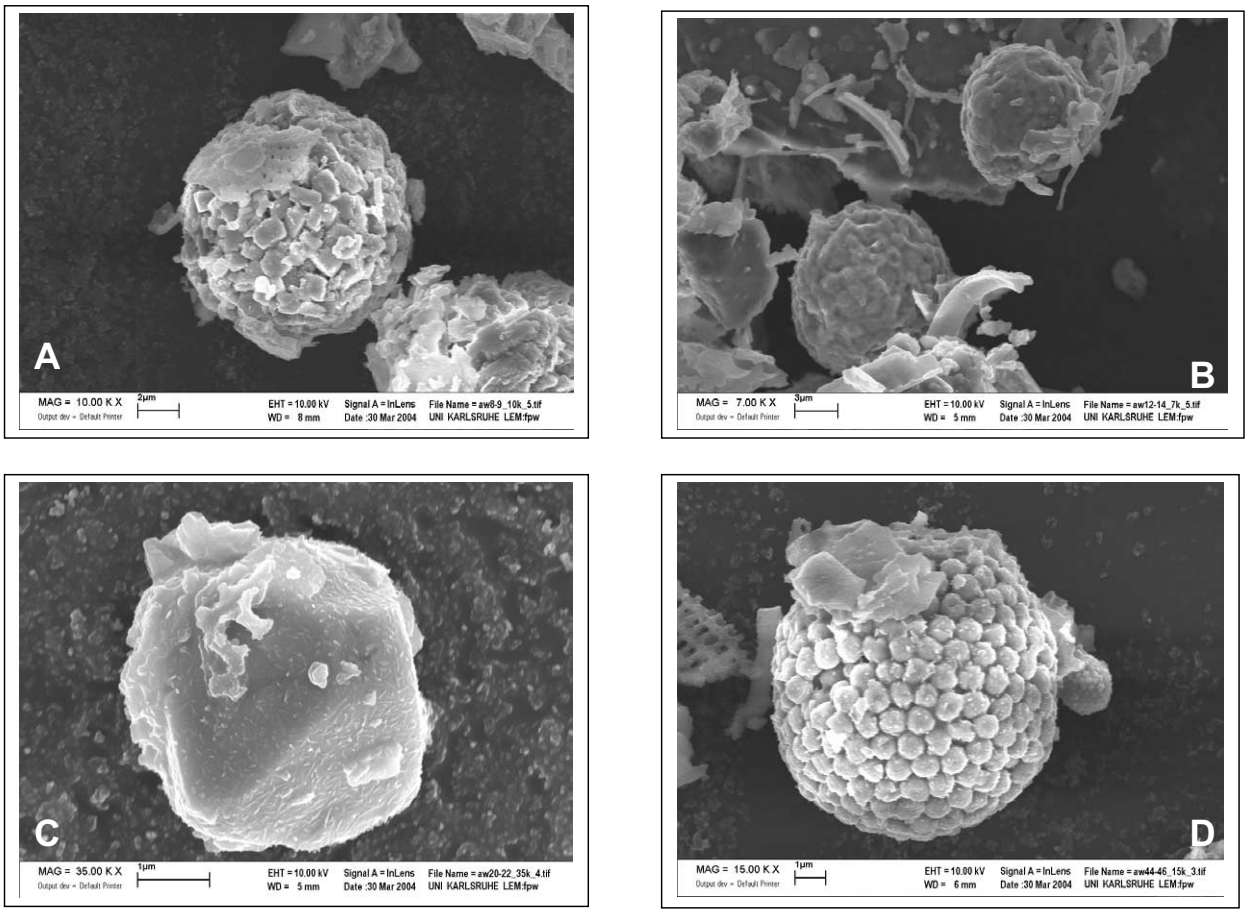

Fig. 2. SEM microphotographs of pyrite from Achterwasser sediments: (A) pyrite framboid at 8–9 cm depth; (B) two pyrite framboids at 12–14 cm depth; (C) euhedral pyrite crystal at 20–22 cm depth; (D) two framboidal pyrite grains with diameters of 1 and 10 μm at 44–46 cm depth.

pyrite mainly occurs as 1 to 20 μm framboidal grains in units II and III, and few euhedral grains are also visible (Fig. 2).

Geochemical analyses of bulk sediment provide a general overview about the composition of the investigated core. For the terrigenous components (K, Ti, Ce, Sc, Y, Zr) a division in only two sections could be seen. In Figure 3 typical depth profiles of Ti and Ce vs. Al are shown. The normalization to Al was chosen to eliminate dilution effects caused by clay minerals. While in the upper part of the core (units I and II) an almost uniform composition is observed, the lower part (unit III) shows higher and more variable Ti/Al- and Ce/Al-ratios. The subdivision into two sections is also seen in Ca/Al- and Sr/Al-ratios due to the presence of carbonate in the upper units I and II of the core.

As seen in enrichments of heavy metals like Cd, Pb, and Tl this upper part of the core is distinctly influenced by anthropogenic activities (Fig. 3). The depth interval between 8 and 25 cm shows especially high enrichments, whereas the uppermost sediment samples reveal a slight decrease in heavy metal contents. This finding is in accordance with measurements of stable Pb isotope ratios that are also presented in Figure 3. While the lower part of unit III (>30 cm) reflects a background with $^{206/207}$Pb ratios of ~1.20–1.23 (Elbaz-Poulichet et al., 1986; Hinrichs et al., 2002), the upper part (unit II) shows a trend towards the anthropogenic and atmospheric signal of 1.11–1.14 (Kersten et al., 1992). Again the uppermost section of unit I shows a very slight increase of $^{206/207}$Pb ratios.

Redox-sensitive trace metals vary in the different units of the core as well (Fig. 3). Mn shows a distribution almost similar to that of Ca, which is most likely due to the formation of Ca-rich rhodochrosite. In contrast, Mo and U are distinctly enriched in an upper interval of unit II (4–10 cm). As Mo and U are ubiquitous trace elements in seawater (Bruland, 1983; Martin and Whitfield, 1983), such enrichments are often observed in TOC-rich deposits, which are influenced by brackish waters (e.g., Dellwig et al., 2002). While Mo forms stable sulfides and/or is incorporated into pyrite under reducing conditions (e.g., Belzile and Lebel, 1986), U shows a strong relation with organic matter (e.g., Cheshire et al., 1977). On the other hand, V follows the distribution of the terrigenous components.

Total inorganic carbon (TIC) shows concentrations of 3.7 wt% near the sediment surface and decreases with depth to 0.3 wt%, whereas the total organic carbon (TOC) contents vary between 6.0 and 10.0 wt% within the entire depth profile (Fig. 4). The total sulfur content ranges from 0.6 to 1.4 mmol/g (2.0 to 4.4 wt%) with lowest values in unit I and highest values at 13 cm depth (Fig. 4).

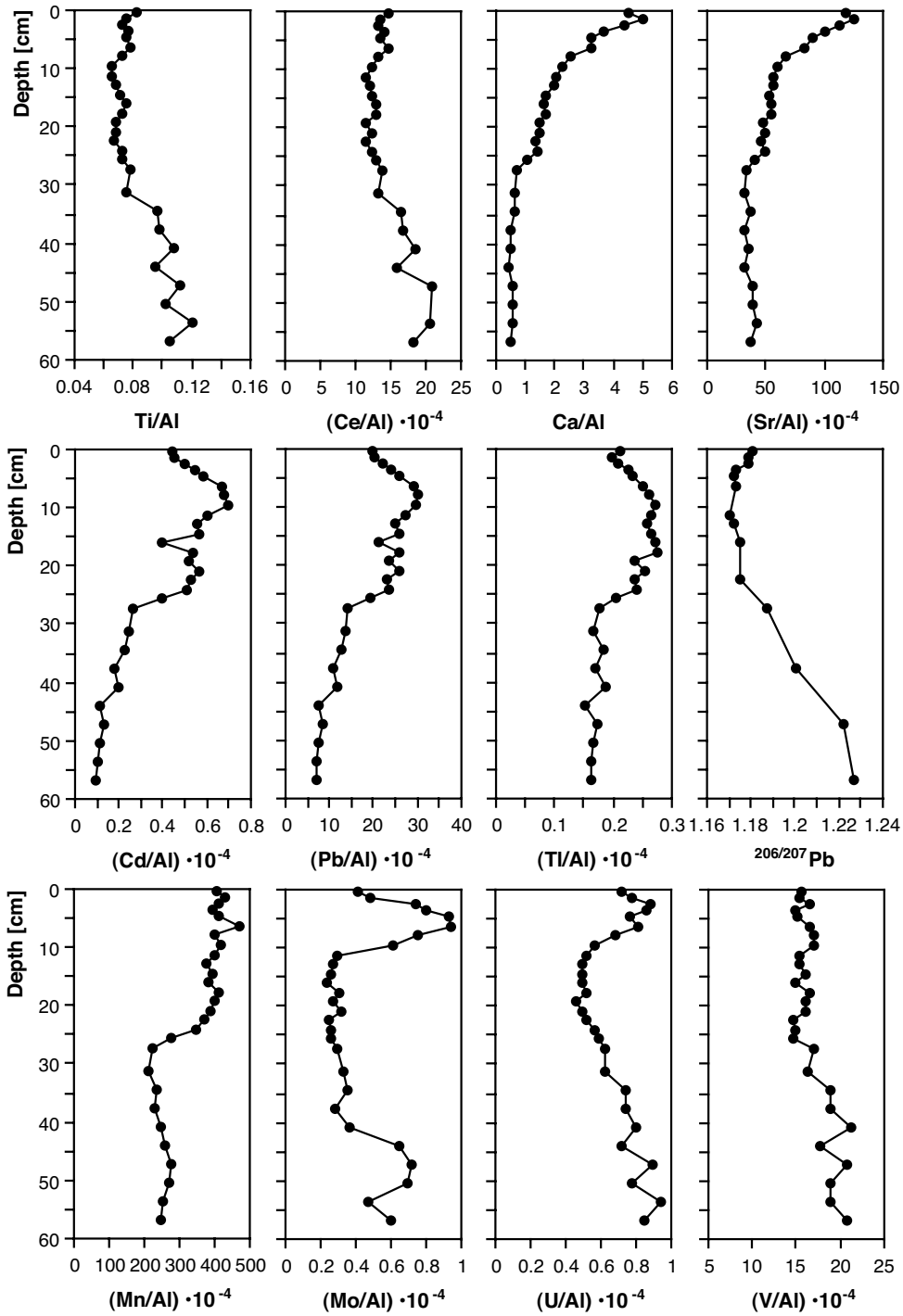

Fig. 3. Depth distribution of element/Al ratios and $^{206/207}$Pb-isotope ratios in sediments of the Achterwasser.

Total Fe concentrations increase with depth from 0.40 mmol/g near the sediment surface to 1.00 mmol/g at 47 cm depth, whereas the behavior of reactive- and pyrite-Fe is more distinct in the different units of the sediment core (Fig. 4). After a strong increase in pyrite-Fe within the upper 13 cm (from 0.20 to 0.62 mmol/g), a sharp decrease to 0.35 mmol/g occurs at a depth of 29 cm. This depth distribution is similar to that of sulfur and corresponds to a maximum pyrite concentration of 7.5 wt% at 13 cm depth. In contrast to pyrite-Fe, the reactive-Fe contents are very low (40 μmol/g) in units I and II. In unit III the reactive-Fe concentration increases to 200 μmol/g at 37 cm depth. DOP values shown in Figure 4 illustrate once again the great difference in the behavior of iron within the various units of the sediment core. In unit II, the DOPs are very high and reach above 90%, whereas unit III is distinguished by moderate DOPs of ~70%.

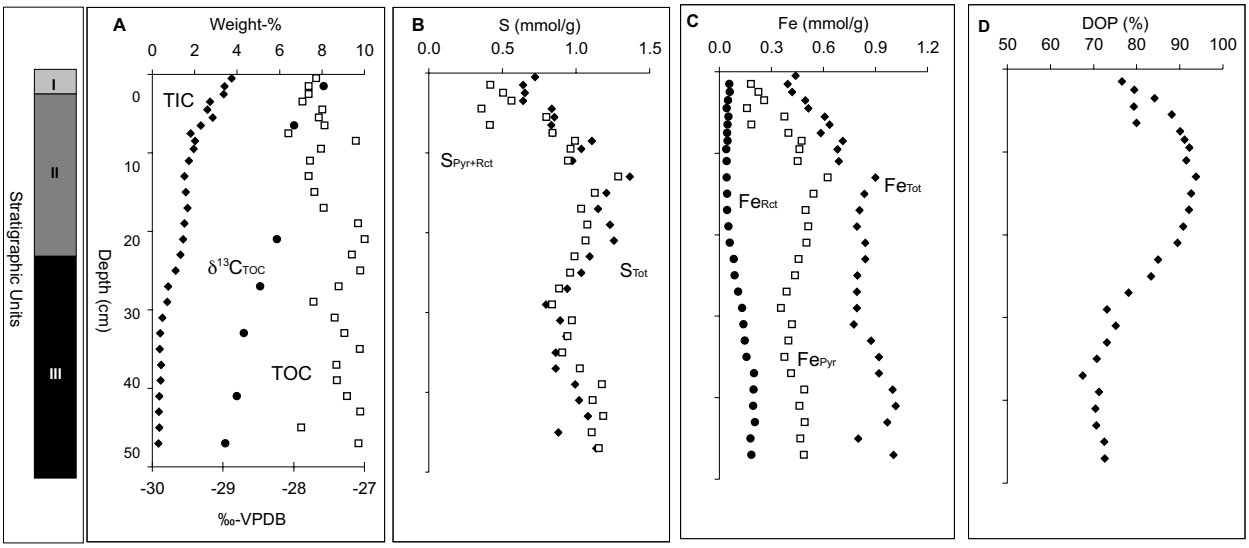

Fig. 4. Depth distribution of TIC (♦), TOC (□), S_{total} (♦), $S_{pyrite+reactive}$ (□), Fe_{total} (♦), Fe_{pyrite} (□), $Fe_{reactive}$ (●), and degree of pyritization (DOP) in sediments of the Achterwasser. The stratigraphy is illustrated on the left side.

4.2. Pore Waters

The chloride concentration in pore water of ~30 mmol/L is almost constant along the whole profile (Fig. 5) and corresponds to a salinity of ~2 in the bottom water of the Achterwasser. The sulfate concentrations decreased from 2.1 mmol/L at the sediment surface to values below 0.1 mmol/L at 27 cm depth and deeper (Fig. 5). Considering sulfate as a conservative constituent in seawater, the sulfate concentration in water with salinity of 2 is 1.6 mmol/L. The sulfate excess of 0.5 mmol/L within unit I may be explained by recycling of sulfur during sulfide oxidation due to penetration of oxic waters into the surficial sediments. Consequently, oxidation of organic matter by sulfate started at 1.6 mmol sulfate per liter below unit I at 3 cm depth. This is also indicated by a continuous increase in H_2S from 0.01 mmol/L to 0.29 mmol/L in unit II and a rapid pH-decrease with depth from 8.4 to 7.1 due to organic matter

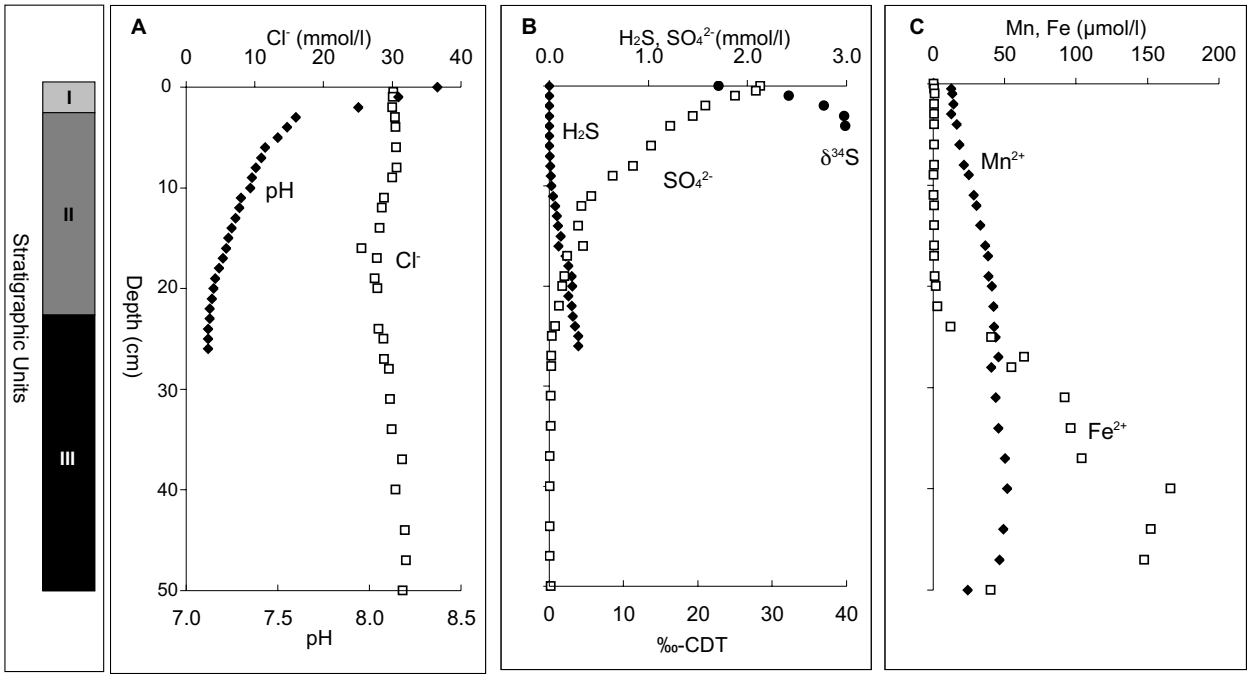

Fig. 5. Depth distribution of Cl^- (□), pH (♦), SO_4^{2-} (□), H_2S (♦), $\delta^{34}S_{SO4}$ (●), Mn(II) (♦), and Fe(II) (□) in pore waters of the Achterwasser. The stratigraphy is illustrated on the left side.

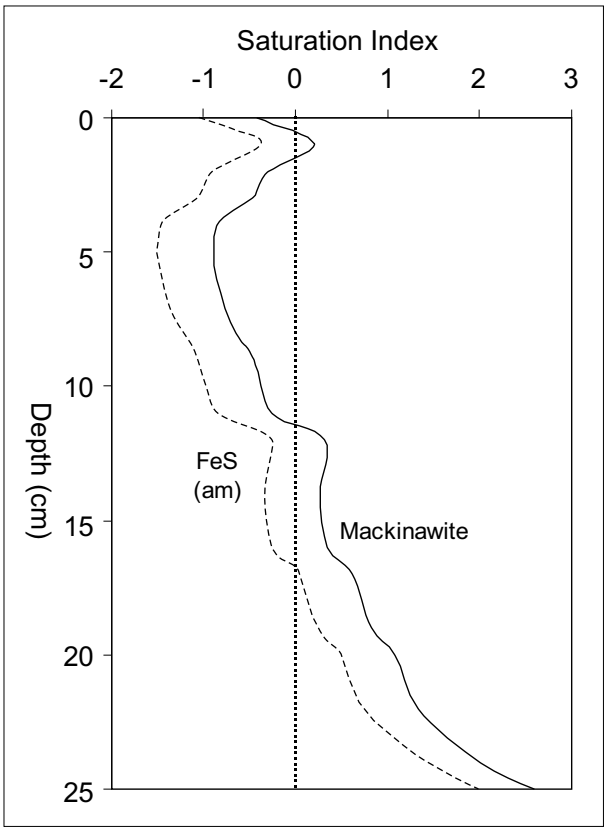

Fig. 6. Saturation indices of pore waters as a function of depth with respect to Fe(am) and mackinawite.

decomposition, especially in the uppermost centimeter of the sediment column (Fig. 5).

The reduction of sulfate affects also the sulfur isotopic composition of dissolved sulfate (Fig. 5) (e.g., Kaplan and Rittenberg, 1964). At the sediment/water interface sulfate show $\delta^{34}S$ values of + 22.7‰, which is close to the isotopic signature of sulfate present in the Baltic Sea (Böttcher and Huckriede, 1997). The rapid increase of $\delta^{34}S$ values to about + 40‰ between 2 and 5 cm depth is typical for ongoing bacterial sulfate reduction. Anaerobic bacteria split oxygen from sulfate ions and release H_2S enriched in ^{32}S whereas the residual sulfate is enriched in ^{34}S.

The rapid change from oxygenated to reduced conditions in the surficial sediments of the Achterwasser is also indicated by the depth distribution of redox sensitive elements, like Mn and Fe (Fig. 5). Dissolved Mn(II) increases from the top (12 μmol/L) to the bottom (50 μmol/L) of the sediment profile reflecting the reduction of Mn oxides during oxidation of organic matter. On the other hand, dissolved Fe(II) concentrations are very low ($<$ 1.0 μmol/L) in units I and II, but increase with depth to a maximum of $\sim$166 μmol/L at 40 cm depth. As free hydrogen sulfide is present, the Achterwasser sediments could be designated as anoxic-sulfidic (Huerta-Diaz and Morse, 1992).

Saturation indices of pore waters with respect to FeS(am) and mackinawite are plotted against depth (Fig. 6). The calculations show that the precursor phases for pyrite formation, such as FeS(am) (SI = $-$1.4 to +0.5) and mackinawite (SI = $-$0.8 to +0.9), are close to saturation within the upper 20 cm of the sediment column and are supersaturated below (SI_{FeSam} = +0.8 to +2.0, $SI_{mackinawite}$ = +1.1 to +2.6).

5. DISCUSSION

5.1. Pyritization of Achterwasser sediments

In comparison to similar low-sulfate coastal environments with anoxic-sulfidic sediments, Achterwasser sediments reveal unexpected high pyrite concentrations (up to 7.5 wt%). For example, sediments of the Baffin Bay contain less than 0.9 wt% pyrite (Huerta-Diaz and Morse, 1992), similar to that reported from the Danube delta (Wijsman et al., 2001). Brüchert and Pratt (1999) investigated anoxic-sulfidic estuarine sediments from northern Florida and found maximum pyrite concentrations of 1.5 wt%. Consequently, less of the reactive-Fe is left in the Achterwasser sediment. The consumption of reactive-Fe leads to very high DOP values of 80 to 95%, which are more characteristic of euxinic depositional environments such as the Black Sea, where iron is the limiting component for pyrite formation (Raiswell et al., 1988; Calvert and Karlin, 1991; Wijsman et al., 2001).

Pyritization of the Achterwasser sediment is not uniform throughout the investigated sediment column and the highest DOP values in units I and II indicate that pyrite formation appears to be most rapid in this section. The DOP profile is reflected by various other elemental distributions. The upper part of the sediment column is distinguished by high amounts of anthropogenic elements, such as Cd, Pb, Tl and low $^{206/207}Pb$ isotope ratios, and the lower part shows elevated concentrations of terrigenous elements, like Ti, Ce and V. This is a typical pattern for sediments of the Baltic Sea reflecting historical changes, e.g., heavy metal pollution of the estuarine and open Baltic environment during the last 100 yrs (Neumann et al., 1996). Accordingly, changing pyrite concentrations with depth may be due to historical changes in rates of pyrite formation in the sediments. The increase in FeS is probably due to the lack of sulfur species with oxidation states intermediate between sulfate and sulfide to convert the FeS to pyrite, along with the slow break down of less reactive iron sources, e.g., Fe-silicates.

The depth distribution of reactive-Fe leads to the conclusion that part of the iron minerals from river input consists of iron phases not as "reactive" as simulated in the extraction method. Fe-silicates need especially long times to react in sulfidic environments to form pyrite (halftime $>10^5$ years) (Canfield et al., 1992; Wijsman et al., 2001), but are partially extracted in 1 M HCl (Huerta-Diaz and Morse, 1990). As the upper 22 cm of the Achterwasser sediment seems to have been deposited during the last 100 to 200 yrs (Neumann et al., 1998), Fe-silicates could not yet have been converted. The fact that nearly all of the reactive Fe (e.g., FeOOH, $FeCO_3$, FeS and adsorbed Fe) in the upper 22 cm has been transformed to pyrite within 100 to 200 yrs points to optimal conditions for pyrite formation in the Achterwasser. This is in contrast to other rapidly accumulating sedimentary environments like deltas, where high contents of Fe-monosulfides are often found (Middelburg, 1991; Wijsman et al., 2001).

Mass balance calculations indicate that the distribution of total-S and the sum of pyrite-S plus monosulfide-S (stoichiometric calculations from pyrite-Fe and reactive-Fe concentrations, respectively) differ with depth (Fig. 4). Within units I and II, the total sulfur content exceeds the amount of sulfur bound to reactive Fe-sulfides and pyrite. Therefore, sulfur must be present in a non-sulfidic form, e.g., as organic-S and/or gypsum, the latter being identified also by X-ray diffraction analyses. In the lower part of unit III, theoretical sulfur depletion was calculated from the difference of total-S against monosulfide-S and pyrite-S concentrations. This suggests that a part of the reactive-Fe is not present as sulfides and possibly occurs in other forms, such as Fe-oxides or Fe-rich clay minerals, which can be leached with 1 M HCl. Consequently, this leads to the relatively low DOP values of ~70% calculated for unit III compared to high DOPs of 80 to 95% in the upper sediment column.

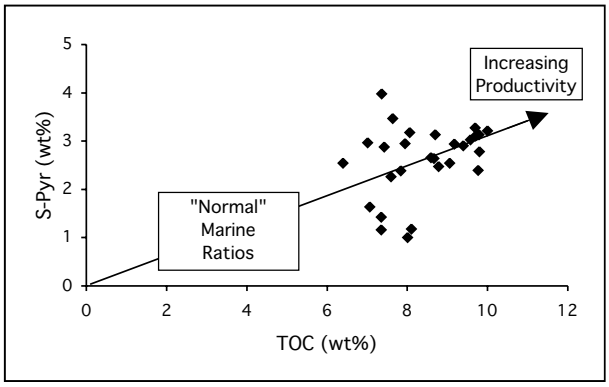

Fig. 7. Plot of organic carbon (TOC) vs. pyritic S (S_{pyr}) for Achterwasser sediments.

5.2. Early Diagenetic Pyrite Formation in Surficial Sediments

The process of sulfate reduction in the surficial sediments of the Achterwasser is clearly reflected by the decrease of dissolved sulfate that is accompanied by an increase in hydrogen sulfide with increasing depth (Fig. 5). Compared to seawater signatures, the elevated $\delta^{34}S$-values of dissolved sulfate in pore water that is close to the sediment surface suggests that the reduction of sulfate is taking place faster than sulfate can be replenished from the overlying water column (e.g., Jørgensen et al., 2004).

The distribution of saturation indices within the sediment core indicates that the pore water chemistry in the surficial sediments is controlled by Fe-monosulfides, such as amorphous FeS and mackinawite (Fig. 6). This is consistent with other field observations and laboratory experiments demonstrating pyrite formation via metastable iron monosulfides (e.g., Schoonen and Barnes, 1991b; Wilkin and Barnes, 1996; Rickard and Luther, 1997; Benning et al., 2000). The inability of pyrite to rapidly nucleate explains high supersaturation with respect to pyrite in anoxic environments (Schoonen and Barnes, 1991a). Although pyrite is the stable Fe-S phase, it will not control the Fe(II) and H_2S concentrations until its growth rate exceeds the dissolution rate of far more soluble, metastable FeS precursor phases.

There are strong indications that pyrite formation near the sediment surface is not limited by the availability of organic matter. Figure 7 plots the TOC content vs. the concentration of pyrite-S. The shift to relatively high TOC and S values compared to oxygenated marine sediments indicates that the sediment accumulation took place in high productivity waters (Calvert and Karlin, 1991). This is supported by the lack of correlation between organic carbon and pyrite-S, which again points to the fact that pyrite formation in the Achterwasser is not limited by the availability of organic matter (Morse and Emeis, 1992). This is in accordance with the present hydrochemical situation of the Achterwasser lagoon showing eutrophic conditions with free oxygen in the entire water column during almost the whole year (Lampe, 1993).

Although dissolved sulfate concentration is relatively low (up to 2.1 mmol/L), H_2S is already available in the Achterwasser sediments. Therefore, sulfate limitation does not seem likely for pyrite authigenesis. An increase of sulfate occurs when brackish Baltic waters with moderate salinity enters the Oder lagoons during high sea levels in the southern Baltic Sea (Lampe, 1993). This results in elevated sulfate concentrations in the Achterwasser and guarantees the availability of sulfate for Fe-sulfide formation.

From our results, we suggest that pyrite formation in the Achterwasser sediments is controlled by (i) the availability of dissolved Fe^{2+}, which limits the FeS formation, and by (ii) the availability of an oxidant, which limits the transformation of FeS into pyrite.

The first step is reflected by the lack of free Fe(II) in pore waters down to the transition of unit II to unit III, the increasing Mn(II) concentrations showing reductive dissolution of oxyhydroxides, and the increasing hydrogen sulfide content with depth. After Canfield and Raiswell (1991) these findings indicate Fe-limited conditions for Fe-sulfide formation.

The ultimate source for reactive-Fe in the Achterwasser is the fluvial input of Fe(III) oxyhydroxides transported by the river Oder. The fraction of unreactive Fe, which is the difference between Fe_{total} and $Fe_{Pyrite+Reactive}$ discharged as suspended matter into the Achterwasser, is only 35%. This value is relatively low compared to the Danube or Dniester deltas which show 60% unreactive Fe (Wijsman et al., 2001). The relatively high fluvial input, ~65% reactive Fe, can be attributed to the contamination of the river Oder by oxidized iron ores from unsafe dumps and insufficiently purified sewage from the Silesian Mining and Industry Area (Helios-Rybicka, 1996). Subsequently, reactive Fe species such as FeOOH will be reduced almost quantitatively to Fe^{2+} in the anoxic sulfidic pore water environment. Coleman and Raiswell (1995) describe this process, where Fe(III) reduction and sulfate reduction occur together, as follows:

$$4FeOOH(s) + 4SO_4^{2-} + 9CH_2O \rightarrow 4FeS(s) + 9HCO_3^- + 6H_2O + H^+ \quad (7)$$

The ultimate limitation for pyrite formation in the Achterwasser is the transformation of FeS to pyrite, which is controlled by the availability of an oxidant to produce sulfur species with intermediate oxidation states. Polysulfides (S_n^{2-}) and thiosul-

fates ($S_2O_3^{2-}$) are then used in the reaction to produce pyrite from Fe-monosulfides (Rickard, 1975; Luther, 1991; Schoonen and Barnes 1991b; Wilkin and Barnes, 1996; Ricard et al., 1995):

$$FeS\ (s) + S_n^{2-} \rightarrow FeS_2(s) + S_{n-1}^{2-} \quad (8)$$

$$FeS\ (s) + S_2O_3^{2-} \rightarrow FeS_2(s) + SO_3^{2-} \quad (9)$$

Reduced Achterwasser surface sediments are subject to oxidizing influences from the overlying water through sediment mixing and pumping. This allows FeS to be rapidly and almost quantitatively converted to pyrite, leaving little FeS and very high DOPs in units I and II. This is in contrast to rapidly accumulating environments, where FeS concentrations can be quite high (Middelburg, 1991; Wijsman et al., 2001) because there is no oxidant to convert them to pyrite.

5.3. Recycling of Fe-Sulfides at the Sediment/Water Interface

The mechanisms and kinetics of FeS_2 and FeS oxidation to produce thiosulfate or polysulfides by O_2, ferric iron, MnO_2 and by bacterial leaching are described by various authors (e.g., Lowson, 1982; Luther, 1987; Moses et al., 1987; Williamson and Rimsted, 1994; Schippers and Sand, 1999; Sand et al., 2001; Schippers and Jørgensen, 2001; Schippers and Jørgensen, 2002). According to the solubility of iron sulfide minerals (Morse et al., 1987; Davison, 1991), amorphous FeS and mackinawite will be dissolved preferentially compared to the more stable mineral pyrite, leading to a relative enrichment of FeS_2 over FeS. Luther (1987) suggested that the initial sulfur products of Fe-sulfide oxidation by O_2 should be thiosulfate, which would slowly react with O_2 to form polythionates and sulfate. According to Schoonen and Barnes (1991b) pyrite formation proceeds at a significant rate only if intermediate sulfur species (i.e., polysulfides, polythionates, or thiosulfate) are present in solution. In the absence of any intermediate sulfur contributor, or with hydrogen sulfide or bisulfide present, FeS_2 formation is much slower. Both processes will enhance pyrite formation according to eqns. (8) and (9).

Shallow water lagoons such as the Oder estuary can be considered as only a temporary sink for particulate matter. Leipe et al. (1998) proposed that the average net sedimentation rate of the Oder estuary is about zero because resuspension and redistribution of surficial sediments in the coastal area, e.g., during strong winds, discharge high amounts of particulate material into the open sea. Resuspension processes and the penetration of oxic bottom waters into the upper anoxic pore water regime lead to partial dissolution of Fe-sulfides. This is indicated by elevated sulfate concentrations in pore waters of unit I above salinities of 2. According to Schippers and Jørgensen (2002), O_2, but not amorphous Fe(III) oxide, is a chemical oxidant for both FeS_2 and FeS in a carbonate-buffered solution at pH 8. This suggests that only O_2, which reacts to form effective oxidizing agents such as H_2O_2 or OH-radical, is responsible for Fe-sulfide dissolution within the surficial pore water environment of the Achterwasser during periodic oxidation events.

As described above intense oxidative dissolution of Fe-monosulfides and subsequent FeS_2 formation occur within the surficial sediment layer. This process may proceed until permanent reduced conditions occur and no more polysulfides or thiosulfates are available for sulfidization of the remaining FeS to pyrite. Therefore, we propose that the process of FeS-recycling at the sediment surface during periodic oxidizing conditions is ultimately responsible for high authigenic pyrite concentrations near the sediment surface, with DOPs between 80 and 95% even under low sulfate conditions.

Framboidal pyrite is the dominant pyrite morphology in the sediments studied, and the size of framboids show variable diameters ranging from 1 to 20 μm. This in accordance with Wilkin et al. (1996), who found that pyrite framboids formed in anoxic sediments underlying a dysoxic or oxic water columns are on average more variable in size than those in the sediments of euxinic basins. The authors proposed that framboid size is related to growth time and rate. In the Achterwasser, with anoxic sediment pore waters underlying an oxic water column, hydrodynamic effects may lead to longer framboid nucleation and growth times compared to euxinic basins.

5.4. Postdepositional Pyrite Formation in the Deeper Sediment Section

The vertical distributions of H_2S, sulfate and Fe^{2+} in pore waters suggest a zone of postdepositional sulfidization at the transition of unit II and III (Fig. 5). While Fe^{2+} is released from reactive-Fe at a depth of 40 to 50 cm, H_2S is produced in measurable concentrations at the lower end of unit II, where the sulfate concentration profile is bent. Unfortunately, the concentration profile of H_2S does not reach deep enough into the sediment to see a decrease of dissolved sulfide at greater depth and thus a flux downward.

According to Allen (2002), a zone of sulfidization occurs when a downward diffusion of H_2S is balanced by an upward migration of Fe^{2+}. Such Liesegang precipitation processes are described as a major cause for sedimentary pyrite formation in laboratory experiments (Allen, 2002), in Black Sea sediments (Jørgensen et al., 2004), and in the Arabian Sea (Schenau et al., 2002). Although the average pyrite concentration in the Arabian Sea is very low (0.4 wt%), the Liesegang precipitation can lead to a major pyrite spike at a certain depth within the sediment profile and to a diagenetic overprint of the pyrites formed at an earlier stage at the sediment surface.

Models of pyritization proposed by Canfield and Raiswell (1991) suggest that the location and extent of pyrite precipitation along a Fe^{2+}/H_2S diffusion front are primarily controlled by the ratio of the reservoir concentrations of Fe and H_2S, with precipitation moving towards the reservoir of the component with the lower concentration. Accordingly, the depth of the postdepositional sulfidization in Achterwasser sediments is influenced by the ambient H_2S concentration and therefore the rate of sulfate reduction.

During times of elevated sulfate concentration in the Achterwasser, caused by the inflow of brackish waters during high sea levels in the Southern Baltic Sea (Lampe, 1993), sulfate reduction increases and the front of postdepositional sulfidization moves to deeper sediment layers. In contrast, low sulfate conditions accompanied by modest production of H_2S lead to postdepositional pyritization in shallower sediment layers. Consequently, vertical fluctuation of the diffusion front forms a

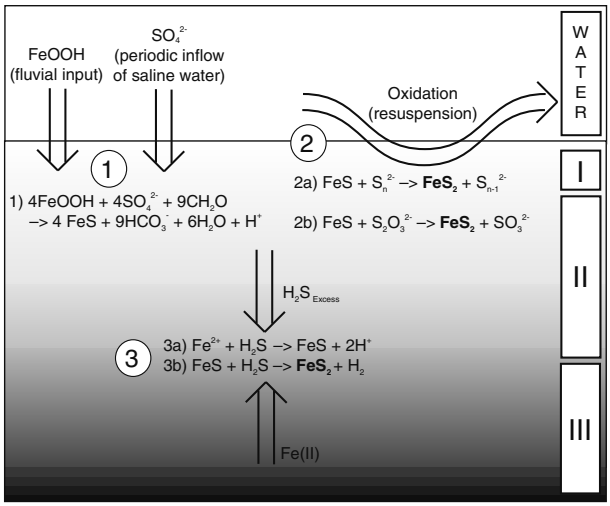

Fig. 8. Model of intense pyrite formation under low sulfate conditions in the Achterwasser lagoon: (1) Early diagenetic formation of Fe-monosulfides below sediment/water interface; (2) Periodic oxidation of surficial sediments (Unit I) enhance pyrite formation; (3) Postdepositional pyritization along a Fe(II)/H_2S-diffusion front at the unit II/III boundary.

layer of postdepositional sulfidization within the profile and intensifies the pyritization of sediments in such environments. Nonetheless, microscopic studies do not show overgrowth on the pyrite grains in Achterwasser sediments. Therefore, we conclude that the postdepositional formation is only of minor importance relative to the early diagenetic pyrite formation close to the sediment surface.

6. CONCLUSIONS

Exceptionally high pyrite concentrations (7.5 wt%) with DOPs of up to 95% in sediments of the Achterwasser lagoon can be explained by early diagenetic formation of Fe-monosulfides and pyrite at the sediment surface and by postdepositional sulfidization at depth (Fig. 8):

1. The formation of Fe-monosulfides at the sediment/water interface is limited by the availability of reactive-Fe. The ultimate source of reactive-Fe is the river Oder, which provides a high portion of reactive-Fe (~65% of the total-Fe). This can be attributed to the contamination of the Oder by oxidized iron ores from unsafe dumps from the Silesian mining area. Subsequently, nearly quantitative reduction of reactive Fe species in the sulfidic pore water environment of the Achterwasser leads to production of Fe-monosulfides.
2. Oxidation of surficial sediments controls the transformation of FeS to FeS_2. The Achterwasser surface sediments are reduced but, through resuspension, are subject to oxidizing influences from the overlying water. Oxidation of the sediments produces sulfur species with oxidation states intermediate between sulfate and sulfide, such as thiosulfate and polysulfides, which transform the remaining FeS to FeS_2 at a significant rate. The process of FeS recycling is thought to be responsible for the formation of authigenic pyrite at high concentrations and DOPs between 80 and 95% even under low sulfate conditions.
3. Postdepositional sulfidization takes place in the deeper part of the sediment core along a front where the downward diffusion of H_2S is balanced by upward migration of Fe(II). The location and extent of this precipitation may be controlled by the rate of sulfate reduction. During times of elevated sulfate concentrations, the front of sulfidization moves to deeper sediment layers, and vice versa. This vertical fluctuation leads to a thick layer of postdepositional pyritization and intensifies the pyritization of sediments in such environments.

Acknowledgments—The authors gratefully acknowledge R. Lampe and H. Meyer from the Institute of Geography at the University of Greifswald for inviting us to join two cruises to the Achterwasser. The crew of R/V Bornhöft provided ideal sampling conditions and is thanked for their commitment to the sampling procedures during the cruises in May and October 2000. MEB wishes to thank J. Rullkötter for the possibility to use the gas isotope mass spectrometer at the ICBM, University of Oldenburg. The authors also thank Associate Editor R. H. Byrne, B. Müller, H. Barnes, I. Butler and one anonymous reviewer for making constructive comments and suggestions, which resulted in significant improvements to this manuscript.

Associate editor: Dr. F. Podosek

REFERENCES

Al-Ahmad H. (1990) Beitrag zur Hydrochemie des Achterwassers. Wiss Z. Ernst-Moritz-Arndt-Universität Greifswald *Math.-nat. Reihe* **39,** 42–45.

Allen R. E. (2002) Role of diffusion—precipitation reactions in authigenic pyritization. *Chem. Geol.* **182,** 461–472.

Aplin A. C. (2000) Mineralogy of modern marine sediments. A geochemical framework. In *EMU Notes in Mineralogy* (eds. D. V. Vaughan and R. A. Wogelius), **Vol. 2/4,** pp. 125–172.

Belzile N. and Lebel J. (1986) Capture of arsenic by pyrite in nearshore marine sediments. *Chem. Geol.* **54,** 279–281.

Benning L. G., Wilkin R. T. and Barnes H. L. (2000) Reaction pathways in the Fe-S system below 100°C. *Chem. Geol.* **167,** 25–51.

Berner R. A. (1970) Sedimentary pyrite formation. *Am. J. Sci.* **268,** 1–23.

Berner R. A. (1984) Sedimentary pyrite formation: An update. *Geochim. Cosmochim. Acta* **48,** 605–615.

Berner R. A. and Raiswell R. (1984) C/S method for distinguishing freshwater from marine sedimentary rocks. *Geology* **12,** 365–368.

Böttcher M. E. and Huckriede H. (1997) First occurrence and stable isotope composition of authigenic γ-MnS in the central Gotland Deep (Baltic Sea). *Mar. Geol.* **137,** 201–205.

Böttcher M. E., Thamdrup B. and Vennemann T. W. (2001) Oxygen and sulfur isotope fractionation during anaerobic bacterial disproportionation of elemental sulfur. *Geochim. Cosmochim. Acta* **65,** 1601–1609.

Brüchert V. and Pratt L. M. (1999) Stable sulfur isotope evidence for historical changes of sulfur cycling in estuarine sediments from northern Florida. *Aquat. Geochem.* **5,** 249–268.

Bruland K. W. (1983) Trace elements in seawater. In *Chem. Oceanography* (eds. J. P. Riley, R. Chester), pp. 157–220. Academic Press London.

Canfield D. E. and Raiswell R. (1991) Pyrite formation and fossil preservation. In *Taphonomy: Releasing the Delta Locked in the Fossil Record* (eds. P. A. Allison and D. E. G. Briggs) vol.9, pp. 337–387. Topics in Geobiology

Canfield D. E., Raiswell R. and Botrell S. (1992) The reactivity of sedimentary iron minerals towards sulfide. *Amer. J. Sci.* **29,** 818–834.

Calvert S. E. and Karlin R. E. (1991) Relationships between sulphur, organic carbon and iron in the modern sediments of the Black Sea. *Geochim. Cosmochim. Acta* **55,** 2483–2490.

Cheshire M. V., Berrow M. L., Goodman B. A. and Mundie C. M. (1977) Metal distribution and nature of some Cu, Mn and V complexes in humic and fulvic acid fractions of soil organic matter. *Geochim. Cosmochim. Acta* **41,** 1131–1138.

Coleman M. L. and Raiswell R. (1995) Source of carbonate and origin of zonation in pyritiferous carbonate concretions: Evaluation of a dynamic model. *Am. J. Sci.* **295,** 282–308.

Davison W. (1991) The solubility of iron sulphides in synthetic and natural waters at ambient termperature. *Aquat. Sci.* **53,** 309–327.

Davison W. and Harbinson T. R. (1988) Performance testing of pH electrodes suitable for low ionic strength solutions. *Analyst* **113,** 709–713.

Dellwig O., Böttcher M. E., Lipinski M. and Brumsack H.-J. (2002) Trace metals in Holocene coastal peats and their relation to pyrite formation (NW Germany). *Chem. Geol.* **182,** 423–442.

Elbaz-Poulichet F., Holliger P., Martin J. M. and Petit D. (1986) Stable lead isotopes ratios in major french rivers and estuaries. *Sci. Tot. Environ* **54,** 61–76.

Gingele F. X. and Leipe T. (1997) Clay mineral assemblages in the western Baltic Sea: recent distribution and relation to sedimentary units. *Marine Geol.* **140,** 97–115.

Govindaraju K. (1994) Compilation of working values and samples description for 383 geostandards. *Geostand. Newsl.* **18**, (special issue) 1–158.

Heinrichs H., Brumsack H.-J., Loftfield N. and König N. (1986) Verbessertes Druckaufschluβsystem für biologische und anorganische Materialien. *Z. Pflanzenernähr. Bodenk.* **149,** 350–353.

Helios-Rybicka E. (1996) Impact of mining and metallurgical industries on the environment in Poland. *Appl. Geochem.* **11,** 3–9.

Hinrichs J., Dellwig O. and Brumsack H.-J. (2002) Pb in sediments and SPM of the German Bight: natural versus anthropogenic origin. *Appl. Geochem.* **17,** 621–632.

Huerta-Diaz M. A. and Morse J. W. (1990) A quantitative method for determination of trace metal concentrations in sedimentary pyrite. *Mar. Chem.* **29,** 119–144.

Huerta-Diaz M. A. and Morse J. W. (1992) Pyritization of trace metals in anoxic marine sediments. *Geochim. Cosmochim. Acta* **56,** 2681–2702.

Jørgensen B. B., Böttcher M. E., Lüschen H., Neretin L. N. and Volkov I. I. (2004) Anaerobic methane oxidation and a deep H2S sink generate isotopically heavy sulfides in Black Sea sediments. *Geochim. Cosmochim. Acta* **68,** 2095–2118.

Kaplan I. R. and Rittenberg S. C. (1964) Microbiological fractionation of sulphur isotopes. *J. Gen. Microbiol.* **34,** 195–212.

Kersten M., Förstner U., Krause P., Kriews M., Dannecker W., Garbe-Schönberg C.-D., Höck M., Terzenbach U. and Graβl H. (1992) Pollution source reconnaissance using stable lead isotope ratios (^{206}/^{207}Pb). In *Impact of heavy metals on the environment* (ed. J.-P. Vernet) pp. 311–325. Elsevier, Amsterdam.

Lampe R. (1993) Environmental state and material flux in the western part of the Oder river estuary—results and consequences. *Peter. Geogr. Mitt.* **137,** 275–282.

Leipe T., Eidam J., Lampe R., Meyer H., Neumann T., Osadczuk A., Janke W., Puff T., Blanz T., Gingele F. X., Dannenberger D. and Witt G (1998) The Oderhaff (Szczecin)—Reconstruction of the Holocenen geological development and anthropogenic impact. *Meer. Ber.* **28,** 61 pp.

Lowson R. T. (1982) Aqueous oxidation of pyrite by molecular oxygen. *Chem. Rev.* **82,** 461–497.

Luther G. W. III. (1987) Pyrite oxidation and reduction: Molecular orbital theory considerations. *Geochim. Cosmochim. Acta* **51,** 3193–3199.

Luther G. W. III. (1991) Pyrite synthesis via polysulfide compounds. *Geochim. Cosmochim Acta* **55,** 2839–2849.

Lyons T. W. and Berner R. A. (1992) Carbon-sulfur-iron systematics of the uppermost deep-water sediments of the Black Sea. *Chem. Geol.* **99,** 1–27.

Martin J. M. and Whitfield M. (1983) The significance of the river input of chemical elements to the ocean. In *Trace metals in sea water* (eds. C. S. Wong, E. Boyle, K. W. Bruland, J. D. Burton and E. D. Goldberg) pp. 265–296. Plenum, New York.

Middelburg J. J. (1991) Organic carbon, sulfur and iron in recent semi-euxinic sediments of Kau Bay, Indonesia. *Geochim. Cosmochim. Acta* **55,** 815–828.

Morse J. W. and Emeis K. C. (1992) Carbon/sulphur/iron relationships in upwelling sediments. *Geol. Soc. Spec. Publ.* **64,** 247–255.

Morse J. W., Millero F. J., Cornwell J. C. and Rickard D. (1987) The chemistry of the hydrogen sulfide and iron sulfide systems in natural waters. *Earth-Sci. Rev.* **24,** 1–42.

Moses C. O., Nordstrom D. K., Herman J. S. and Mills A. L. (1987) Aqueous pyrite oxidation by dissolved oxygen and ferric iron. *Geochim. Cosmochim. Acta* **51,** 1561–1571.

Müller B (1996) ChemEQL—A computer program to calculate chemical equilibria. Online publication http://www.eawag.ch/research/surf/forschung/chemeql.html.

Neumann T., Leipe T., Brand T. and Shimmield G. (1996) Accumulation of heavy metals in the Oder estuary and its off-shore basins. *Chemie Erde* **56,** 207–222.

Neumann T. Leipe T. and Shimmield G. (1998) Heavy-metal enrichment in surficial sediments in the Oder River discharge area: source or sink for heavy metals. *Appl. Geochem.* **13,** 329–337.

Niemistö L. (1974) A gravity corer for studies of soft sediments. *Merentutkimuslait. Julk/Havsforskningsinst. Skr.***238,** 33–38.

Pohl C., Hennings U., Petersohn I. and Siegel. H (1998) Trace metal budget, transport, modification and sink in the transition area between the Oder and Peene Rivers and the Southern Pomeranian Bight. Bull. *Mar. Poll. Bull.* **36** (*8*), 598–616.

Raiswell R. and Berner R. A. (1985) Pyrite formation in euxinic and semi-euxinic sediments. *Am. J. Sci.* **285,** 710–724.

Raiswell R., Buckley F., Berner R. A. and Anderson T. F. (1988): Degree of pyritization as a paleoenvironmental indicator of bottom water oxygenation. *J. Sediment. Petrol.* **58,** 812–819.

Rickard D. T. (1975) Kinetics and mechanisms of pyrite formation at low temperatures. *Am. J. Sci.* **275,** 636–652.

Rickard D. (1997) Kinetics of pyrite formation by the H_2S oxidation of iron (II) monosulfide in aqueous solutions between 25 and 125°C: The rate equation. *Geochim. Cosmochim. Acta* **61,** 115–134.

Rickard D. and Luther G. W. III. (1997) Kinetics of pyrite formation by the H_2S oxidation of iron (II) monosulfide in aqueous solutions between 25 and 125°C: The mechanism. *Geochim. Cosmochim. Acta* **61,** 135–147.

Rickard D., Schoonen M. A. A. and Luther G. W. III. (1995) The chemistry of Fe sulfides in sedimentary environments. In *Geochemical Transformations of Sedimentary Sulfur* (ed. V. Vairavamurthy and M. A. A. Schoonen), Vol. 612, Chap. 9, pp. 168–193. American Chem. Society Symposium Series.

Sand W., Gehrke T., Jozsa P.-G., Schippers A. (2001) (Bio)chemistry of bacterial leaching—Direct vs. indirect bioleaching. *Hydrometall.* **59,** 159–1175.

Schelske C. L. and Hodell D. A. (1991) Recent changes in productivity and climate of Lake Ontario detected by isotopic analysis of sediments. *Limnol. Oceanogr.* **36** (*5*), 961–975.

Schenau S. J., Passier H. F., Reichart G. J. and de Lange G. J. (2002) Sedimentary pyrite formation in the Arabian Sea. *Mar. Geol.* **185,** 393–402.

Schippers A. and Jørgensen B. B. (2001) Oxidation of pyrite and iron sulfide by manganese dioxide in marine sediments. *Geochim Cosmochim Acta* **65,** 915–922.

Schippers A. and Jørgensen B. B. (2002) Biogeochemistry of pyrite and iron sulfide oxidation in marine sediments. *Geochim. Cosmochim. Acta* **66,** 85–92.

Schippers A. and Sand W. (1999) Bacterial leaching of metal sulfides proceeds by two indirect mechanisms via tiosulfate or via polysulfides and sulfur. *Appl. Env. Microbiol.* **65,** 319–321.

Schoonen M. A. A. and Barnes H. L. (1991a) Reactions forming pyrite and marcasite from solution: I. Nucleation of FeS2 below 100°C *Geochim. Cosmochim. Acta* **55,** 1495–1504.

Schoonen M. A. A. and Barnes H. L. (1991b) Reactions forming pyrite and marcasite from solution: II. Via FeS precursors below 100°C *Geochim. Cosmochim. Acta* **55,** 1505–1514.

Stumm W. and Morgan J. J. (1996) Aquatic Chemistry. Wiley, New York, N. Y. 1022 pp.

Vaughan D. J. and Craig J. R. (1978) Mineral Chemistry of Metal Sulfides. Cambridge University Press, New York, N. Y., 493 pp.

Wijsman J. W. M., Middelburg J. J. and Heip C. H. R. (2001) Reactive iron in Black Sea sediments: implications for iron cycling. *Mar. Geol.* **172,** 167–180.

Wilkin R. T. and Barnes H. L. (1996) Pyrite formation by reaction of iron monosulfides with dissolved inorganic and organic sulfur species. *Geochim. Cosmochim. Acta* **60,** 4167–4179.

Wilkin R. T., Barnes H. L. and Brantly S. L. (1996) The size distribution of framboidal pyrite in modern sediments—an indicator of redox conditions. *Geochim. Cosmochim. Acta* **60,** 3897–3912.

Williamson M. A. and Rimstidt J. D. (1994) The kinetics and electrochemical rate-determining step of aqueous pyrite oxidation. *Geochim. Cosmochim. Acta* **58,** 5443–5454.

ELECTRONIC ANNEX

Supplementary data associated with this article can be found, in the online version, at doi:10.1016/j.gca.2005.02.034.